

Corrosion Behaviour of Weathering Steel with High-Content Titanium Exposed to Simulated Marine Environment

Lei Weng, Linxiu Du^{*}, Hongyan Wu,

The State Key Laboratory of Rolling and Automation, Northeastern University, Shenyang 110819, Liaoning, China.

*E-mail: ralwenglei@163.com ; dulx@ral.neu.edu.cn

Received: 28 Decemebr 2017 / *Accepted:* 31 March 2018 / *Published:* 10 May 2018

In this work, cyclic immersion experiments were carried out to study the corrosion behaviour of high-Ti weathering steel exposed to a simulated marine environment. The corrosion behaviour of high-Ti weathering steel was characterized by corrosion kinetics, surface morphology of corrosion products and electrochemical techniques. The results indicate that protective corrosion products are formed on the surface of the high-Ti weathering steel sample, improving the corrosion resistance. Corrosion potential (E_{corr}) of high-Ti weathering steel rises with increased corrosion time, and the corrosion current density (I_{corr}) varies little after the formation of the corrosion products. The presence of titanium promotes the formation of dense and compact corrosion products, promoting improved corrosion resistance.

Keywords: corrosion behaviour; marine environment; weathering steel; titanium; electrochemistry

1. INTRODUCTION

Weathering steel containing Cu, P, Cr, Ni, and Si as alloying elements is one of the important steels used for anti-corrosion materials. Generally, in a practical operational environment, adherent, compact, and protective corrosion products are formed on the steel surface, retarding further corrosion [1]. Cu, P, Cr and Ni are common anti-corrosion alloying elements that are widely considered to improve the corrosion resistance of steels by the formation of protective corrosion products [2]. In recent years, the exploitation and utilization of marine resources has attracted intense interest worldwide [3]. Weathering steel, as the main material of marine engineering structures, has become particularly important owing to the continuous marine development. Many researchers have focused on the development and improvement of cost-effective materials ranging from Cu-P addition weathering steel to Cr-Ni weathering steel [4-11]. For example, Misawa [12] studied the role of alloying elements on corrosion behaviour and noted that Cu and P are enriched in the inner layer. Hao

[13] found that weathering steel containing Mn, Cu and P shows outstanding corrosion resistance in a simulated coastal atmosphere, and the amount of the goethite (α -FeOOH) corrosion product in the rust layer increases with the progress of the corrosion process. Cr and Ni are effective elements for improving the corrosion resistance of steel. However, the reserves of Cr and Ni in China are extremely poor. By contrary, China is well-known to contain abundant of Ti reserves. Titanium is often used to improve mechanical properties of steel through the precipitate strength effect. The study of Liu [14] demonstrated that titanium is beneficial for the formation of compact and dense corrosion products in low-alloy steel. Thus, elemental titanium has a positive effect on the corrosion resistance. Nevertheless, currently, there are few reports in the literature on the weathering steel with a high titanium element content. Therefore, it is highly necessary to study the corrosion behaviour of weathering steel with the addition of a high titanium content exposed to simulated marine environment as well as the role of titanium in the formation of the corrosion products.

To investigate the role played by titanium in the formation of the corrosion products, [Ishikawa](#) [15-21] carried out a series of studies on the influence of metal ion on ferric oxyhydroxides (α -FeOOH, β -FeOOH and γ -FeOOH) and magnetite (Fe_3O_4) by using the artificial synthetic colloid method. The artificially synthesized goethite (α -FeOOH) is one of the most thermodynamically stable corrosion products. The crystallite size of α -FeOOH increases with the Ti(IV) addition, which promotes the formation of double domain particles of α -FeOOH core and porous poorly crystalline shell. Akaganeite (β -FeOOH) is one of the typical corrosion products of steel formed in the corrosion environment with a high content of Cl^- ions, such as the marine atmosphere. Ti(IV) also influences the crystallization and particle growth of β -FeOOH. The Ti(IV)-containing steel raises the corrosion resistance. The crystal structure and particle size of the lepidocrocite (γ -FeOOH) corrosion product are not obviously influenced by Ti(IV). The corrosion products formed owing to the addition of Ti(IV) exhibit superparamagnetism at room temperature and the blocking temperature decreases. Furthermore, the local structure of the corrosion products was influenced by Ti(IV) owing to the replacement of Fe(III) by Ti(IV). Electrochemical measurement is a common approach for the investigation of the corrosion products' characteristics. The electrochemical properties of the corrosion products influence the corrosion resistance. Thus, the corrosion behaviour of steel is widely characterized by using electrochemical experiments [22-24].

In summary, studies on the impact of titanium on the corrosion behaviour of weathering steel containing high titanium content are rare, and the corrosion mechanism of the weathering steel with high added titanium content has been seldom reported. In this paper, the corrosion behaviour of designed high titanium content weathering steel is studied by using wet/dry accelerated corrosion experiments to simulate a marine environment.

2. EXPERIMENTAL PROCEDURE

2.1 Materials and solution

The chemical compositions of the designed steels are listed in Table 1. For comparison, a carbon steel widely used in industrial was also studied in order to elucidate the effect of titanium on the corrosion resistance.

Table 1. Chemical composition of tested steels (mass %)

Elements	C	Si	Mn	P	S	Al	Cu	Ti	Fe
High-Ti weathering steel	0.03	0.29	0.99	0.099	0.005	0.03	0.351	0.2	Balance
Carbon steel	0.17	0.19	1.06	0.015	0.006	0.027	0.025	-	Balance

The designed steel was melted with a vacuum furnace, cast into an ingot and forged into a plate with the thickness of 80 mm. The plate was reheated at 1200 °C for 2 h and rolled into steel plates with the thickness of 6 mm through seven passes by a rolling mill. The finishing rolling temperature was 900 °C. The steel plate was cooled to 650 °C by water, which was the cooling temperature in the industrial fabrication process. The rolled steel was then slowly cooled to room temperature in a furnace. The steel plates were cut into two kinds of specimens with the dimensions of 60 mm × 40 mm × 5 mm and 22 mm × 20 mm × 5 mm. These two kinds of specimens were used for the determination of the corrosion loss and for morphology observation, respectively. Then, the exposed surfaces were polished by SiC papers successively up to 1000# grade. Prior to the corrosion experiments, the specimens were cleaned in petroleum ether, alcohol and acetone to remove the dust and grease on the specimens and then were dried using cold air. The weight of the specimens with the dimensions of 60 mm×40 mm× 5 mm were measured by using an electronic balance with the accuracy of 0.1 mg.

2.2 Experimental process

Following the specifications in the ASTM G44-99 standard [25], cyclic alternate immersion experiments were carried out to simulate a marine environment. The electrolyte was a 3.5 mass% NaCl solution. The water used in this experiment was distilled and NaCl was used as the analytical reagent. Air temperature and relative humidity are important factors that affect the corrosion process. The air temperature was 45 ± 2 °C and the relative humidity of air was 70 ± 5 % throughout the entire experimental process. The duration of a single cycle is 60 minutes. During the wet cycle process, the samples were immersed in the electrolyte solution for 12 minutes. During the dry cycle process, these samples were exposed to environmental air for 48 minutes. The accelerated corrosion experiment was carried out for 360 h, and the samples were removed from the solution after 72 h, 144 h, 216 h, 288 h and 360 h cyclic alternate immersion, respectively. The corrosion products were removed by the chemical method. The cleaning solution consisted of 500 mL 37 vol % hydrochloric acid, 500 mL reagent water and 3.5 g hexamethylene tetramine. The initial weight (m_1) of each specimen was obtained after washing and drying. The final weight (m_2) of each specimen after the removal of the corrosion products was recorded again using an electronic balance. The preparation process of the examined samples, such as cleaning, and weight-loss was based on the ASTM G1-03 [26]. The average corrosion rate (CR) was obtained according to the equation (1):

$$\text{Corrosion Rate} = (K \times W) / (A \times T \times D) \quad (1)$$

Where K is the corrosion rate constant evaluated in mm/y and is found to be 8.76×10^4 , W is the mass loss in g calculated as $W = m_1 - m_2$, A is the exposed surface area of the tested specimens in cm^2 , T is the corrosion time in h and D is the steel density in g/cm^3 .

2.3 Electrochemical experiments

The square of the samples used for open circuit potential (OCP) and electrochemical polarization measurements was 78.5 mm^2 (diameter of 10 mm). The wires were welded on the sample surface. All tested samples were embedded by using epoxy resin and only the specific surfaces were exposed for corrosion. The exposed surfaces of each sample were mechanically polished with 1000# SiC paper. All tested samples were cleaned in acetone and ethanol by ultra-sonication and dried by cold air. Subsequently, the cleaned samples were stored in a desiccator prior to the cyclic alternate immersion experiments.

A three-electrode system consisting of the samples as the working electrode (WE), saturated calomel electrode with Luggin capillary as the reference electrode (SCE), and platinum plate as the counter electrode (CE) were used for measurements. OCP values of two bare steels were recorded using a potentiostat in a 3.5 mass% NaCl solution. For each electrochemical experiment, the steel reached a relatively steady-state value. Simultaneously, the variation of the self-corrosion potential with the immersion time was monitored and recorded. After the cyclic accelerated corrosion experiment, the polarization curves measurements were carried out on the corroded samples. Prior to the experiment, the working electrode was immersed in a 3.5 mass% NaCl solution and the steel reached a relatively steady-state OCP value. The potentiodynamic polarization experiment was performed from -200 mV to 200 mV (vs SCE) with the scan rate of 0.5 mV/s. All electrochemical experiments were carried out using a CS350 workstation at the temperature of 25 °C.

2.4 Corrosion products characterization

The morphology characteristics of the corrosion products on the tested samples formed after different cycle times were observed by an FEI QUANTA 600 scanning electron microscope (SEM). X-ray diffraction (XRD) measurements with $\text{Co}_{K\alpha}$ and the step of 0.04° were carried out to study the corrosion products. The XRD scan was carried out for angles ranging from 10 to 80° , and the obtained patterns of the corrosion products were matched by using the MDI Jade software with database PDF-2 (2004).

3. RESULTS AND DISCUSSION

3.1 Microstructure

Fig. 1 shows the microstructure morphologies of the high-Ti weathering steel and the carbon steel. Examination of the optical microscopy (OM) and SEM images (Figs. 1a and 1c, respectively) show that the microstructure of the high-Ti weathering steel consists of quasi-polygonal ferrite with fine grains. The grain size of the high-Ti weathering steel was measured by using image analysis software and the average grain size was found to be approximately $3.34 \mu\text{m}$. Figs. 1b and 1d reveal that the microstructure of carbon steel is ferrite and pearlite. The average grain size of carbon steel is approximately $4.88 \mu\text{m}$.

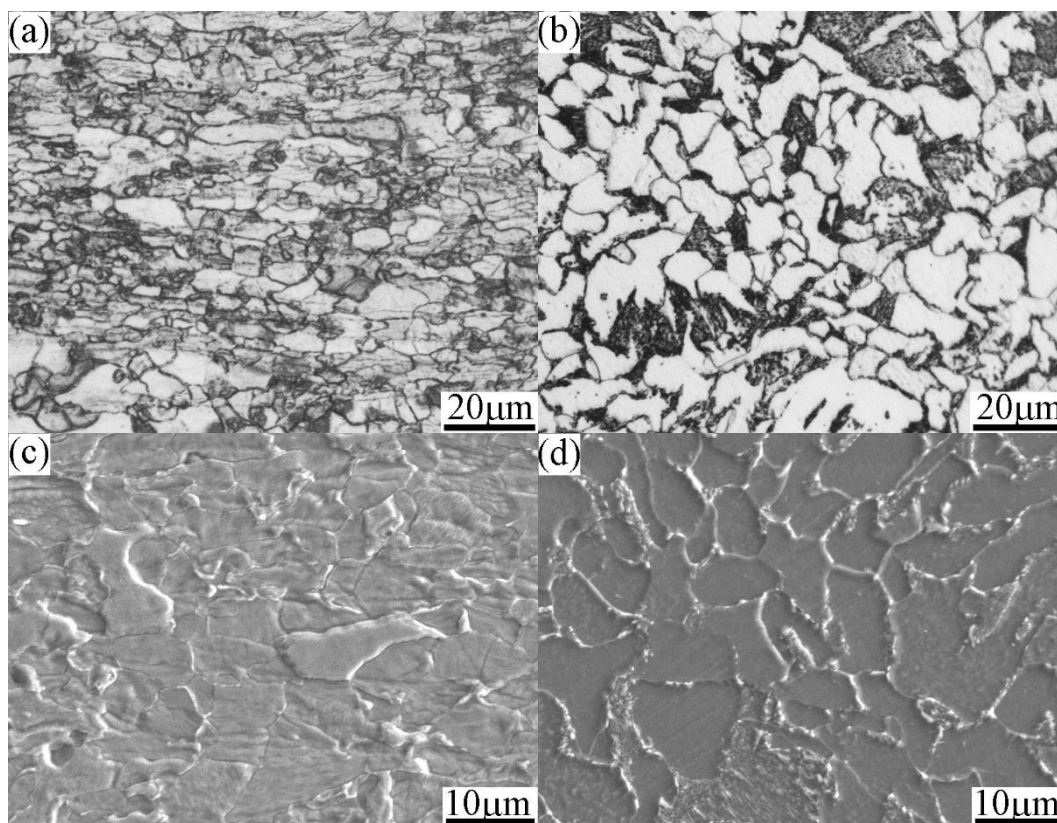


Figure 1. Microstructure morphology of the high-Ti weathering steel (a and c) and the carbon steel (b and d): (a) and (b) OM images; (c) and (d) SEM images.

3.2 Corrosion kinetics curves

Table 2. Corrosion rate of the high-Ti weathering steel and the carbon steel (mm/y)

Corrosion time	72 h	144 h	216 h	288 h	360 h
High-Ti weathering steel	7.20	5.83	4.53	4.46	3.97
Carbon steel	7.32	6.90	6.08	6.12	5.56

Table 2 shows the trend of the changes in the corrosion rate with the increasing corrosion time. It was shown that the corrosion rate of the high-Ti weathering steel and carbon steel decreases with longer corrosion time. The corrosion rate of the high-Ti weathering steel is lower than that of carbon steel, indicating that the corrosion resistance of the designed weathering steel is better than that of carbon steel. The final experimental corrosion rate value of the designed weathering steel is 3.97 mm/y. Thus, the data in Table 2 demonstrate that the addition of high titanium content improves the corrosion resistance.

The curves of the weight loss with increasing corrosion time are shown in Fig. 2. The corrosion process of the weathering steel is clearly divided into two stages according to the curves of the weight loss. But this change of carbon steel cannot be obviously distinguished. Initially, (0-72 h), the weight loss of the high-Ti weathering steel and the carbon steel were similar. In the subsequent corrosion process, the weight loss of the designed weathering steel changes mildly and that of carbon steel

increases sharply, indicating that the corrosion resistance of the designed weathering steel is better than that of carbon steel. Many studies [13, 27, 28, 29] show that, the different stages of corrosion model correspond to different controlling mechanism. In this study, the first stage is a linear function of time. The anodic dissolution of steel and the cathodic reduction of dissolved oxygen dominate corrosion process. With the corrosion progressing, the corrosion products were formed with time until they reaches certain density or thickness. These corrosion products hinder the dissolved oxygen to the steel surface in the second stage. Then, the cathodic reduction is dominated.

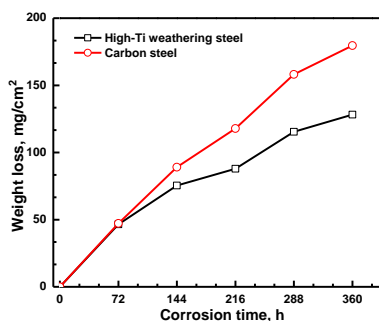


Figure 2. The weight loss of two samples steel at different corrosion time (solution of 3.5 mass % NaCl, temperature of 45 °C, humidity of 70%, immersion time of 12 minutes, dry time of 48 minutes)

3.3 Surface morphologies

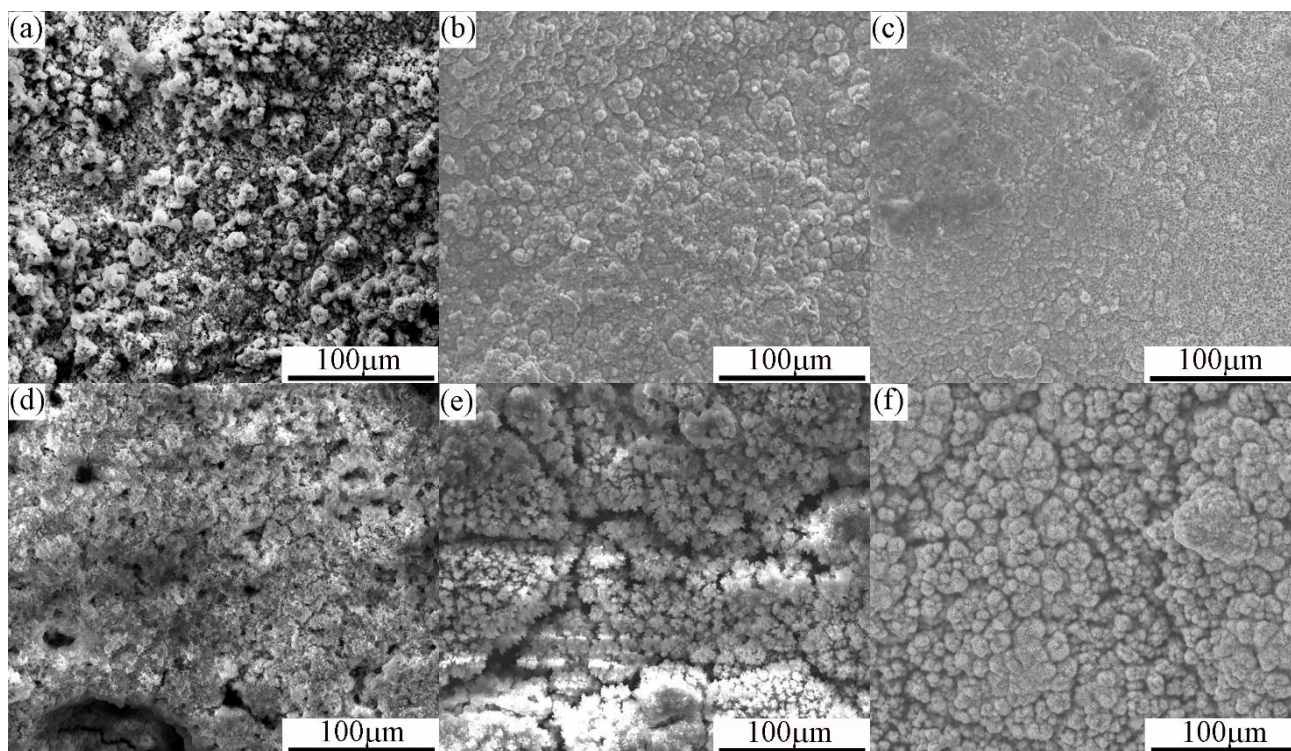


Figure 3. Microscopic surface morphologies of corrosion products of the high-Ti weathering steel (a-c) and the carbon steel (d-f) after different immersion times, (a) and (d) 72 h, (b) and (e) 216 h and (c) and (f) 360 h, respectively (solution of 3.5 mass % NaCl, temperature of 45 °C, humidity of 70%, immersion time of 12 minutes, dry time of 48 minutes).

Fig. 3 shows the morphology characteristics of the corrosion products formed on the specimen surface of the high-Ti weathering steel and carbon steel after immersion for 72 h, 216 h and 360 h. Fig. 3a shows that the granular corrosion products cover the surface of the high-Ti weathering steel specimen after corrosion for 72 h. With increasing corrosion time (Fig. 3b), the structure of the corrosion products on the sample surface becomes fine and compact, improving the corrosion resistance owing to the decrease in the diffusion channel. Fig. 3e reveals that the morphology of the corrosion products of the high-Ti weathering steel surface is small and dense. The corrosion products completely cover the entire sample surface, and no cracks and holes were found on the sample surface. The thick and dense corrosion products promotes corrosion resistance because the ion transfer resistance is increased [30, 31]. In this study, the corrosion products formed on the surface of designed weathering steel show the globular (“cotton balls”) structures, typical morphology of goethite (α -FeOOH), and the globules (sandy crystals) structures, typical morphology of lepidocrocite (γ -FeOOH). The typical morphologies of the corrosion products was reported in many studies [32, 33]. Figs. 3a-c show that corrosion products become denser with the increasing corrosion time. Thus, the corrosion rate decreases gradually (as shown in Table 2).

For carbon steel, Fig. 3d shows that corrosion products do not completely cover the sample surface and no protective corrosion products are formed on the sample surface, which is unfavourable for the corrosion resistance because the corrosive ions in the electrolyte solution can easily diffuse into the steel substrate. There are obvious cracks and holes on the surface, and the compactness at the initial stage of corrosion is poor. When the number of corrosion cycles increases (Fig. 3e), the defect density of holes and cracks decreases obviously, and the corrosion products become compact. However, the crack of the corrosion products is still obviously observed. In Fig. 3f, the particles of corrosion products were coarse and loose on the carbon steel surface. The density of the carbon steel corrosion products is obviously lower than that of the high-Ti weathering steel. Corrosion products morphologies showed a “rosette” shape. This is a typical appearance of akaganeite (β -FeOOH) [32, 33]. Fig. 3 demonstrates that the structure of the corrosion products formed on the sample surface of the high-Ti steel is more compact and dense than that of carbon steel. In general, the corrosion resistance of metal is affected by the corrosion products on the metal surface. The dense corrosion products improve the corrosion resistance owing to the smaller density of the capillaries. Thus, the corrosion rate of the high-Ti steel is lower than that of carbon steel (Table 2).

3.4 XRD analysis

Fig. 4 shows the XRD patterns of the corrosion products formed on designed steel and carbon steel after different cyclic alternate immersion times. Fig. 4a shows that the amount of corrosion products of the high-Ti weathering steel does not change significantly with increasing corrosion time. The corrosion products are mainly α -FeOOH, γ -FeOOH and Fe_3O_4 . Fig. 4b shows that the corrosion products of carbon steel also consist of α -FeOOH, γ -FeOOH, Fe_3O_4 and especially β -FeOOH. However, the corrosion products peak intensity of carbon steel showed obvious differences at 72 h and

later cycles as seen in Fig. 4(b). The special relative peak intensity appears to be due to akaganeite ($2\theta = 13.76^\circ$). This is because carbon steel does not produce stable corrosion products at the initial stage.

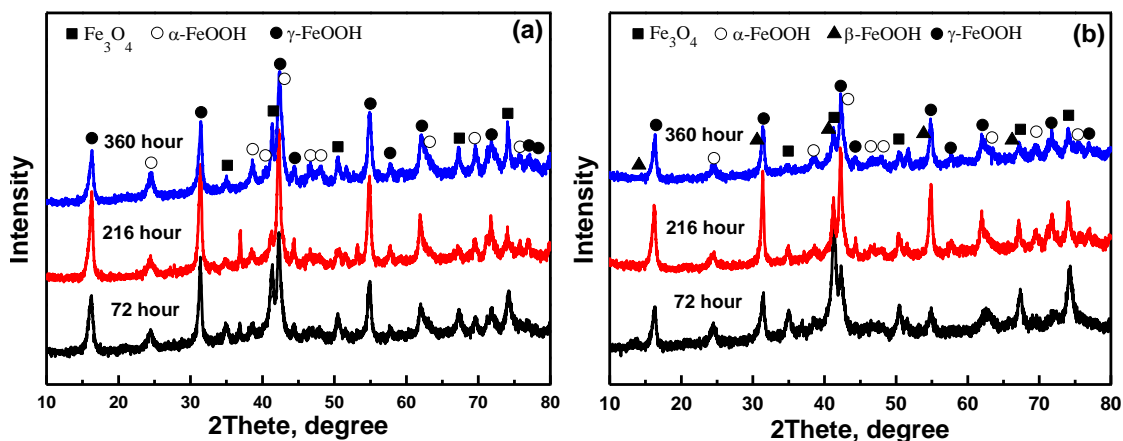


Figure 4. XRD patterns of corrosion products of the high-Ti weathering steel and the carbon steel after different cyclic alternate immersion times (a) high-Ti weathering steel and (b) carbon steel (solution of 3.5 mass % NaCl, temperature of 45 °C, humidity of 70%, immersion time of 12 minutes, dry time of 48 minutes).

After 72 h corrosion, there is a great difference in the peak intensity positions between the high-Ti weathering steel and carbon steel. The pattern of the corrosion products of high-Ti weathering steel shows the highest intensity peaks for α -FeOOH and γ -FeOOH. By contrast, for carbon steel the highest intensities are observed for the Fe_3O_4 and β -FeOOH peaks. This indicates that after 72 h corrosion during the cyclic alternate immersion test, high-Ti weathering steel rapidly generates protective properties corrosion products, contributing to the addition of alloy elements. The corrosion products exhibit poor corrosion resistance because no alloying elements are added to the carbon steel. It is accepted that the corrosion products are blocked by the presence of chloride ions. The porous structure of β -FeOOH provides the transmission channels for the chloride ions [34]. Nishimura's study [35] demonstrates the possibility that β -FeOOH is easily produced by the electrochemical reaction for the steel. This result suggests that β -FeOOH also accelerates the corrosion in the initial wet/dry stage as it works as a cathode [36]. Thus, the corrosion rate of carbon steel is higher than that of high-Ti weathering steel.

After 360 h corrosion, the corrosion products of high-Ti weathering steel and carbon steel were similar. Although the XRD pattern of corrosion products of high-Ti weathering steel and carbon steel both show the presence of α -FeOOH and γ -FeOOH, the diffraction peak intensities of high-Ti weathering steel are higher than those of carbon steel. In high-Ti weathering steel, the diffraction intensity of Fe_3O_4 decreases slightly with the increasing the cycle time. However, the diffraction intensity of α -FeOOH increases slightly with increasing cycle time. The origins of this phenomenon are discussed in detail in the following section.

3.5 Electrochemical analysis

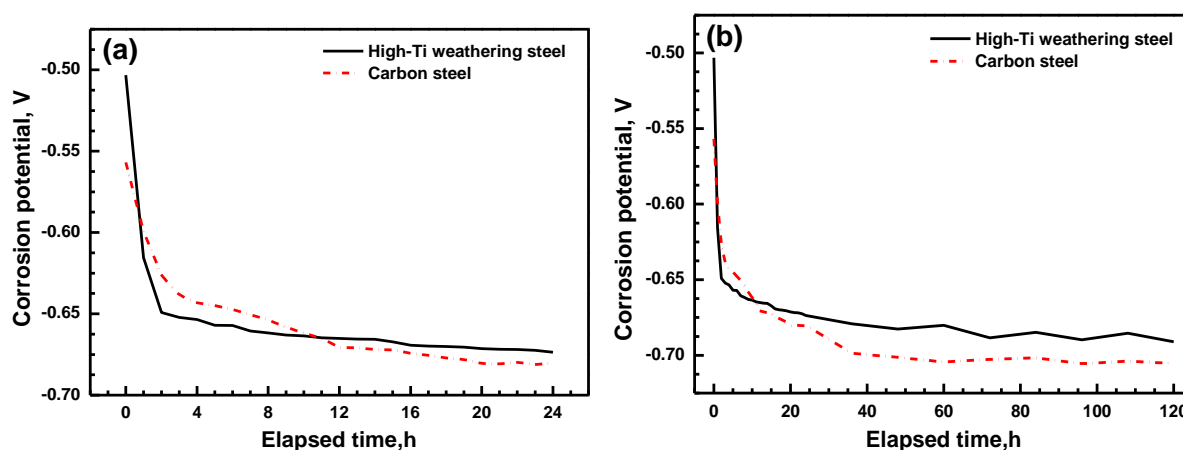


Figure 5. Time dependence of the OCP of two bare steels: (a) 24 h and (b) 120 h (solution of 3.5 mass% NaCl, temperature of 25 °C)

Fig. 5 shows the results of the OCP for two bare steel samples immersed in a 3.5 mass% NaCl aqueous solution with pH 7.0 at 25 °C. As shown in Fig. 5a, the OCP suddenly drops during the initial 4 h. The slope of high-Ti weathering steel is larger than that of carbon steel and the time required to reaching the knee point OCP of high-Ti weathering steel is also shorter than that of carbon steel. The time required to reach the OCP knee point for the high-Ti weathering steel is approximately 2 h, where it is approximately 2.5 h for carbon steel. The knee point value of high-Ti weathering steel is approximately -0.65 V (vs SCE). Fig. 5b shows that the OCPs of high-Ti weathering steel and carbon reached steady values after approximately 40 h corrosion. The OCP values of high-Ti weathering steel and carbon steel are approximately -0.69 V and -0.71 V respectively. The Eoc value of weathering steel is higher than that of carbon steel, demonstrating that the more thermodynamic stable high-Ti weathering steel is less prone to corrosion.

3.6 Potentiodynamic polarization

The potentiodynamic polarization curves of two bare steels (high-Ti weathering steel and carbon steel) are shown in Fig. 6. Table 3 shows the electrochemical parameters of the polarization curves of two bare steel. The corrosion potentials of high-Ti weathering steel and carbon steel after Tafel fitting are -0.45 V and -0.50 V, respectively. The corrosion potential of the designed weathering steel is higher than that of carbon steel. The corrosion current density of weathering steel is less than that of carbon steel by an order of magnitude. On the two bare steels, the cathode behaviour is controlled by the diffusion limit of dissolved oxygen, and the anodic reaction consists of the dissolution of iron and controlled by the charge transfer [13, 27, 37].

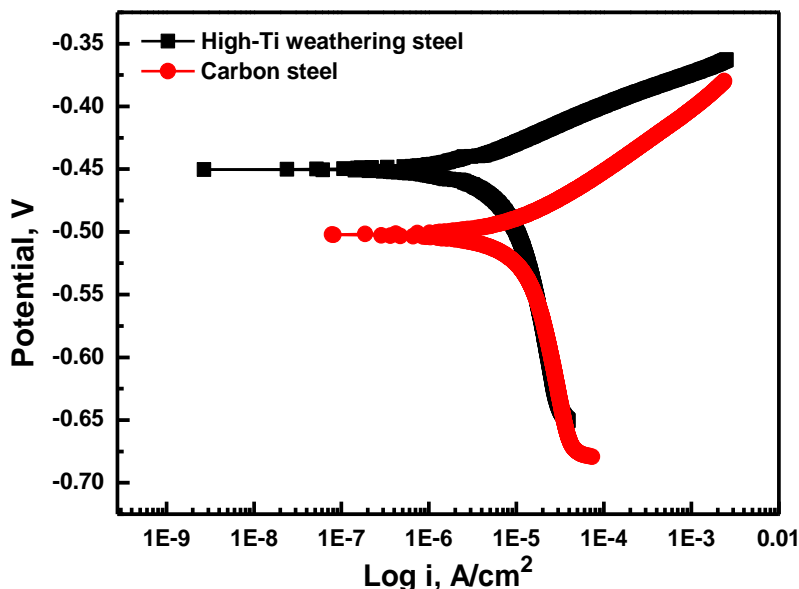


Figure 6. Potentiodynamic polarization curves of two bare steels samples (solution of 3.5 mass% NaCl, temperature of 25 °C).

Table 3. The electrochemical parameters of polarization curves of two bare steel

Sample	Time/h	b_a (mV/dec)	b_c (mV/dec)	E_{corr} (V)	I_{corr} (A/cm ²)
High-Ti weathering steel	0	35	-195	-0.45	3.27×10^{-6}
Carbon steel	0	52	-295	-0.50	1.20×10^{-5}

The potentiodynamic polarization curves of high-Ti weathering steel and carbon steel after different corrosion time are shown in Fig. 7. The corrosion potentials of both high-Ti weathering steel and carbon steel rise with increasing corrosion time. However, the corrosion current density of both steels changes little. Nevertheless, their corrosion resistance value are different because the regulation of the potentiodynamic polarization curves reveals a great difference. Fig. 7a shows that the corrosion potential of the high-Ti weathering steel increases slightly with the corrosion process. The corrosion potential of carbon steel is divided into two stages (Fig. 7b). In the first stage, the corrosion products are formed on the samples surface and completely cover the surface after 72 h immersion. The corrosion process is inhibited by these corrosion products. However the corrosion products contain voids and cracks which do not effectively prevent the corrosion ions from accessing the steel substrate. In the second stage, the corrosion products' thickness increases with increasing corrosion time. The corrosion potential reaches a stable state after 216 h. Although voids and cracks are still present on the surface of carbon steel, the corrosion process is obviously suppressed owing to the thickening of the corrosion products.

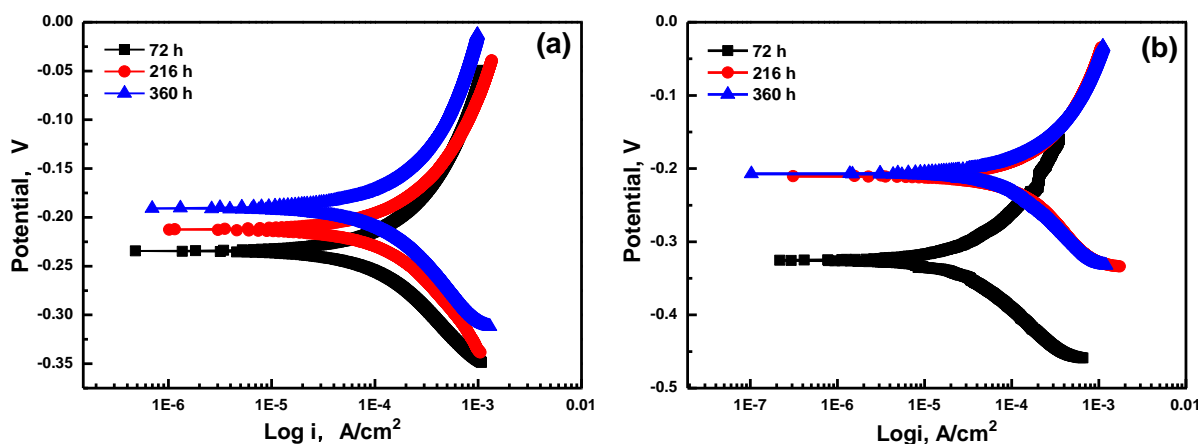


Figure. 7. Potentiodynamic polarization curves of different steels formed at the corrosion environment (solution of 3.5 mass% NaCl, temperature of 45 °C, humidity of 70%, immersion time of 12 minutes and dry time of 48 minutes) tested in 3.5 mass% NaCl solution and at 25 °C. (a) the high-Ti weathering steel and (b) the carbon steel

Table 4. The electrochemical parameters of polarization curves of designed weathering steel and carbon steel

Sample	Time/h	b_a (mV/dec)	b_c (mV/dec)	E_{corr} (V)	I_{corr} (A/cm ²)
High-Ti weathering steel	72	141	-149	-0.234	1.51×10^{-4}
	216	138	-158	-0.212	1.85×10^{-4}
	360	160	-148	-0.191	1.70×10^{-4}
Carbon steel	72	126	-126	-0.326	3.86×10^{-5}
	216	206	-226	-0.21	2.55×10^{-4}
	360	195	-203	-0.207	1.90×10^{-4}

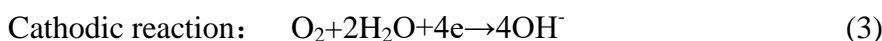
Both anodic and cathodic branches of the potentiodynamic polarization curves indicate the Tafel relationship characteristics for the corrosion products formed after different immersion times. Thus, Tafel extrapolation can be used to calculate the corrosion kinetics' parameters. The corresponding anodic slope (b_a), cathodic slope (b_c), corrosion potential (E_{corr}), and corrosion current density (I_{corr}) are given in Table 4. The corrosion potential is shifted in the positive direction. According the mathematical models [38], it is evident that the kinetic behaviour of metal materials is under activation control. Thus, the Tafel extrapolation of anode and cathode are controlled by activation. After the formation of stable corrosion products, the corrosion current density is almost unchanged with increasing corrosion time. For the designed weathering steel and carbon steel, the change of anodic slope and cathodic slope is not obvious when the rust layer is covered. These electrochemical parameters show that the weathering steel has better corrosion resistance.

3.7 Corrosion process

Based on the results of XRD analysis, surface morphology and potentiodynamic polarization curve, it can be inferred that the addition of titanium element improves the corrosion resistance of the

designed weathering steel. The corrosion evolution of steel includes many reaction at different corrosion stages.

In a simulated marine environment, the corrosion process of bare steel is an electrochemical corrosion process. The corrosion process consists of two parts: anode and cathode. For the surface of bare steel, the anodic dissolution of steel and the cathodic reduction of dissolved oxygen dominate the corrosion process [13, 27, 28, 29], as indicated in Fig. 6. The electrochemical dissolution of metal materials is controlled by charge transfer under anodic polarization behaviour, and the cathodic polarization behaviour is affected by the diffusion limit of dissolved oxygen [37]. At the initial corrosion stage, the equation for the electrochemical corrosion reactions of steel are listed as following equations (2-4):



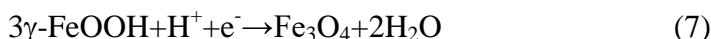
The formation mechanisms of the intermediate corrosion products (green rust one) explain the coexistence of Fe(II)-Fe(III) hydroxyl and Cl^- anions [39, 40]. The existence of Cl^- is conducive to the formation of β -FeOOH, which decreases the corrosion resistance of carbon steel exposed to marine environment and accelerates the corrosion process [11, 36, 40, 41].

As shown in Fig. 4, the peaks of corrosion products formed after 72 h immersion are obviously different. The XRD pattern of corrosion products shows the highest peak intensity of α -FeOOH and γ -FeOOH for the designed weathering steel, where for carbon steel the highest peak intensity is observed for β -FeOOH and Fe_3O_4 peaks. The addition of Ti inhibits the formation and crystallization of β -FeOOH in Cl^- containing environment, improving the corrosion resistance because β -FeOOH is detrimental for corrosion resistance [16, 20, 42]. Moreover, Nishmura [43] found that ultrafine-grained weathering steel had excellent corrosion resistance compared with carbon, which was consistent with the results shown in this study. The addition of Ti precludes austenite growth and the fine grain is obtained after the hot-rolling process [44]. Generally, the FeOH^+ corrosion intermediate products is rapidly oxidized by O_2 to generate γ -FeOOH [45, 46]. Therefore, the corrosion products of the high-Ti weathering steel mainly consist of γ -FeOOH at the early stage of the corrosion process. This reaction is described by formula (5):



γ -FeOOH easily transforms into α -FeOOH by dissolution and reprecipitation in neutral or slightly acidic solutions [11, 47, 48]. α -FeOOH is a thermodynamically stable phase and it is difficult to transform it into other phases during the cathodic reduction process. Evans [49] and Kamimura [36] pointed out that Fe_3O_4 , a good electrical conductor in the rust layer, can be used as a large cathode to accelerate metal corrosion. At the same time, beneficial elements added to the designed weathering steel inhibit the formation of crystalline Fe_3O_4 in the cathodic reduction process [50]. By contrast, carbon steel does not contain the alloying elements. In a chloride-rich environment, the unstable β -FeOOH is formed on large scale during the corrosion process. β -FeOOH is directly converted into Fe_3O_4 , and gradually transforms into the metastable γ -FeOOH. Atmospheric corrosion of steel has been intensely studied by many researchers [47-51]. Upon directly contacting with metal surface or connecting to it through conductive materials, γ -FeOOH transforms into Fe_3O_4 by the electrochemical

cathodic process. The electrochemical reactions of β -FeOOH and γ -FeOOH are expressed by equations (6) and (7).



Reactions (6) and (7) describe the changes of the corrosion kinetics parameters of the designed weathering steel and carbon steel listed in Table 4. After 72 h cyclic alternate immersion, the limited diffusion characteristics of dissolved oxygen of the designed weathering steel gradually disappear in the cathodic process, and the charge transfer control of the reduction of corrosion products gradually becomes dominant. The slope of the cathodic polarization curve decreases and the increase of the corrosion current density is caused by the covering of the corrosion products on the sample surface. The corrosion potential is gradually shifted, and the anodic slope of corresponding polarization curve increases. At this time, the corrosion resistance of the designed weathering steel tends to be stable, and the anodic and cathodic slopes are maintained at constant values in the subsequent cyclic alternate immersion test.

However, the anodic and cathodic corrosion behaviours of carbon steel are affected by the structural characteristics of the corrosion products. The decrease of the anodic slope is caused by the cathodic reduction of β -FeOOH, one of the corrosion products on the sample surface. The decrease of the cathodic slope is caused by the cathodic reduction of the β -FeOOH corrosion product, and the β -FeOOH corrosion product is converted into Fe_3O_4 under a high cathodic potential. The corrosion potential is gradually shifted, and the anodic slope also increases gradually. As shown in Fig. 4 and Table 4, the corrosion products of high-Ti weathering steel and carbon steel are almost the same after 360 h cyclic alternate immersion test. As mentioned above, the corrosion products on the sample surface of the designed weathering steel are basically stable, and the corrosion products are dense and free of holes. Therefore, the corrosion potential increases slightly, and the corrosion current density is almost unchanged.

On the other hand, the amount of the corrosion products of carbon steel gradually increases while their structure remains stable. The anodic polarization is inhibited because of the thickening of the corrosion products and the hindrance to the ions migration. The cathodic polarization is almost unchanged because of the increase in the number of reducible corrosion products. The thickness of the corrosion products increases. The diffusion of dissolved oxygen is blocked, and the dissolved oxygen concentration at the interface of corrosion products and steel substrate decreases. β -FeOOH and γ -FeOOH begin to participate in the cathodic reduction reaction to form stable Fe_3O_4 . The transformation of the corrosion products in different valence states can reach a relative balance. Evans [49] studied the reaction between magnetite (Fe_3O_4) and iron hydroxide oxide (FeOOH), which is described by the shown as following equations:



According to the discussion mentioned above, the mechanism is summarized. At the early stage of the corrosion process (0 h-72 h), before the rust layer is formed on the metal surface, the chloride ion can easily dissolve Fe and form Fe^{2+} as a soluble phase [52]. The corrosion products are related to the alloy elements in the steel and the chloride ion in solution. Many previous studies [20, 40, 41] have

shown that the corrosion products of carbon steel consists of abundant β -FeOOH, and Fe_3O_4 and a small amount of γ -FeOOH when the steel is exposed to the corrosion environment containing Cl^- , which is in good agreement with the present observations (Fig. 4b). In Fig. 4(a), the corrosion products of high-Ti weathering steel are similar to the low alloy steel studied by Misawa [12, 53], and the anticorrosion functionality of Ti for the steels effectively inhibited the formation of β -FeOOH [21].

At the later corrosion stage, the corrosion processes of the two kinds of steel are different. The surface of the high-Ti steel is covered with dense corrosion products, as shown in Fig. 3(a). With the increasing corrosion time, the results of the XRD patterns (Fig. 4a) and E_{corr} (Fig. 7a) changed little, contributing to the reason that the alloy elements promote the formation of dense oxide film, and hinder the migration of Cl^- to the interface of the corrosion products and steel matrix. However, the carbon steel lacks of alloy elements and the corrosion products exhibit a loose structure (Fig. 3d), providing a diffusion channel for corrosive media and oxygen. Thus, the corrosion process occurs continually. After 216 h immersion, the corrosion products film on the steel surface becomes thick and blocks the migration of Cl^- . Consequently, the electrode potential and the structure of the corrosion products are almost stable, as supported by Figs. 7(b) and 4(b). In contrast to the results obtained by Zhou [54], Fe_3O_4 and β -FeOOH convert into γ -FeOOH in the corrosion process and then transform into a thermodynamically stable phase, namely α -FeOOH [55].

Thus, the addition of Ti into steel significantly improves the corrosion resistance and promotes the formation of dense and non-porous protective rust formation.

4. CONCLUSIONS

The electrochemical corrosion behaviour of high-Ti weathering steel and carbon steel were studied in a simulated marine environment. The conclusions obtained from the experimental results can be summarized as follows.

1. After 120 h immersion, the OCP of high-Ti weathering steel is always higher than that of carbon steel. The corrosion potential of the high-Ti weathering steel is improved by the addition of titanium.
2. The corrosion potential (E_{corr}) and corrosion current density (I_{corr}) of the high-Ti weathering steel are higher than those of carbon steel. The high-Ti weathering steel shows an excellent corrosion resistance.
3. The addition of titanium promotes the activation of the weathering steel surface and the formation of dense and compact corrosion products.

References

1. M. Morcillo, I. Díaz, B. Chico, H. Cano, and D. de la Fuente, *Corros. Sci.*, 83 (2014) 6.
2. R.W. Revie, H. H. Uhlig, *Corrosion and Corrosion Control*, John Wiley & Sons, Inc., (2008) New York, U.S.
3. S. Zhang, X. Cheng, L. Su and C. Jiang, *Int. J. Electrochem. Sci.*, 12 (2017) 2453.
4. Y. Xie, Y. Wang and Y. Men, *Int. J. Electrochem. Sci.*, 7 (2012) 10679.
5. S. A. Park, W. S. Ji and J. G. Kim, *Int. J. Electrochem. Sci.*, 8 (2013) 7498.

6. T. Misawa, K. Asami and S. Hashimoto, *Corros. Sci.*, 14 (1974) 279.
7. K. Inouye, K. Ichimura, K. Kaneko and T. Ishikawa, *Corros. Sci.*, 16 (1976) 507.
8. M. Kimura, H. Kihira, N. Ohta and M. Hashimoto, *Corros. Sci.*, 47 (2005) 2499.
9. M. Yamashita, H. Miyuki, Y. Matsuda and H. Nagano, T. Misawa, *Corros. Sci.*, 36 (1994) 283.
10. K. Asami, M. Kikuchi, *Corros. Sci.*, 45 (2003) 2671.
11. D. A. Shifler, *Corrosion and corrosion control in saltwater environments: proceedings of the international symposium*. The Electrochemical Society, Inc., (2000) Pennington, U.K.
12. T. Misawa, T. Kyuno, W. Suëtaka and S. Shimodaira, *Corros. Sci.*, 11 (1971) 35.
13. L. Hao, S.X. Zhang, J. H. Dong and W. Ke, *Corros. Sci.*, 58 (2012) 175.
14. Z. G. Liu, X. H. Gao and L.X. Du, *Int. J. Electrochem. Sci.*, 11 (2016) 6540.
15. T. Ishikawa, H. Yamashita, A. Yasukawa, T. Nakayama and F. Yuse, *J. Mater. Chem.*, 10 (2000) 543.
16. T. Nakayama, T. Ishikawa and T. J. Konno, *Corros. Sci.*, 47 (2005) 2521.
17. T. Ishikawa, R. Katoh, A. Yasukawa, K. Kandori, T. Nakayama and F. Yuse, *Corros. Sci.*, 43 (2001) 1727.
18. T. Ishikawa, M. Kumagai, A. Yasukawa, K. Kandori, T. Nakayama and F. Yuse, *Corros. Sci.*, 44 (2002) 1073.
19. T. Ishikawa, T. Ueno. A. Yasukawa, K. Kandori, T. Nakayama and T. Tsubota, *Corros. Sci.*, 44 (2003) 1037.
20. T. Ishikawa, Y. Kondo, A. Yasukawa and K. Kandori, *Corros. Sci.*, 40 (1998) 1239.
21. T. Ishikawa, T. Motoki, R. Katoh, A. Yasukawa, K. Kandori, T. Nakayama and F. Yuse, *J. Colloid Interface Sci.*, 250 (2002) 74.
22. T. Nishimura, H. Katayama, K. Noda and T. Kodama, *Corrosion*, 56 (2000) 935.
23. B. Naima, M. Bounoughaz and A. Bouklachi, *Int. J. Electrochem. Sci.*, 11 (2016) 215.
24. K. C. R. Ferreira, R. F. B. Cordeiro, J. C. Nunes, H. Orofino, M. Magalhães, A. G. Torres and E. D'Elia, *Int. J. Electrochem. Sci.*, 11 (2016) 406.
25. ASTM G44-99, ASTM International, (2013) West Conshohocken, United States.
26. ASTM G1-03, ASTM International, (2011) West Conshohocken, United States.
27. L. Hao, S.X. Zhang, J. H. Dong and W. Ke, *Corros. Sci.*, 59 (2012) 270.
28. R. E. Melchers and R. Jeffrey, *Corros. Sci.*, 47 (2005) 1678.
29. R. E. Melchers, *Corros. Sci.*, 45 (2003) 923.
30. D.D.L. Fuente, I. Díaz, J. Simancas, B. Chico, M. Morcillo, *Corros. Sci.*, 53 (2011) 604.
31. Y.Y. Chen, H.J. Tzeng, L.I. Wei, L.H. Wang, J.C. Oung, and H.C. Shih, *Corros. Sci.*, 47 (2005) 1001.
32. D. de la Fuente, I. Díaz, J. Simancas, B. Chico, and M. Morcillo, *Corros. Sci.*, 53 (2011) 604.
33. Renato Altobelli Antunes, Isolda Costa, and Dalva Lúcia Araújo de Faria, *Materials Research*, 6 (2003) 403.
34. P. Dhaiveegan, N. Elangovan, T. Nishimura, and N. Rajendran, *Mater. Trans.*, 57 (2016) 148.
35. T. Nishimura, I. Tanaka, Y. Shimizu, *Tetsu-to-Hagane*, 81 (1995) 1079.
36. T. Kamimura, S. Hara, H. Miyuki, M. Yamashita, and H. Uchida, *Corros. Sci.*, 48 (2006), 2799.
37. E. McCafferty, *Corros. Sci.*, 47 (2005) 3202.
38. F. Bolzoni, S. Goidanich, L. Lazzari, M. Ormellese and MP. Pedefferri, Laboratory Testing on the Influence of Alternated Current on Steel Corrosion, *CORROSION/04*, New Orleans, U.S., 2004, Paper 04208.
39. P. Refait and J. M. R. Génin, *Corros. Sci.*, 34 (1993) 797.
40. P. Refait, M. Abdelmoula and J. M. R. Génin, *Corros. Sci.*, 40 (1998) 1547.
41. Y. T. Ma, Y. Li and F. H. Wang, *Corros. Sci.*, 51 (2009) 997.
42. T. Ishikawa, T. Motoki, K. Kandori, T. Nakayama and T. Tsubota, *J. Colloid Interface Sci.*, 265 (2003) 320.
43. T. Nishimura, *Corros. Sci.*, 50 (2008) 1306.

44. R. D. K. Misra, H. Nathani, J. E. Hartmann and F. Siciliano, *Mater. Sci. Eng. A-Struce.*, 394 (2005) 339.
45. Y. Zou, J. Wang and Y. Y. Zheng, *Corros. Sci.*, 53 (2011) 208.
46. Y. T. Ma, Y. Li and F. H. Wang, *Mater. Chem. Phys.*, 112 (2008) 844.
47. M. Yamashita, H. Miyuki, Y. Matsuda, H. Nagano and T. Misawa, *Corros. Sci.*, 36 (1994) 283.
48. S. Hoerlé, F. Mazaudier, P. Dillmann and G. Santarini, *Corros. Sci.*, 46 (2004) 1431.
49. U. R. Evans, and C. A. J. Taylor, *Corros. Sci.*, 12 (1972) 227.
50. I. Suzuki, N. Masuko and Y. Hisamatsu, *Corros. Sci.*, 19 (1979) 521.
51. U. R. Evans, *Nature*, 206 (1965) 980.
52. J.Y. Hu, S.A. Cao, and J.L. Xie, *Anti-Corrosion Methods and Materials*, 60 (2013) 100.
53. T. Misawa, K. Hashimoto and S. Shimodaira, *Corros. Sci.*, 14 (1974) 131.
54. Y.L. Zhou, J. Chen, Y. Xu, and Z.Y. Liu, *J. Mater. Sci. Technol.*, 29 (2013) 168.
55. S. J. Oh, D. C. Cook, and H. E. Townsend, *Corros. Sci.*, 41 (1999) 1687.

© 2018 The Authors. Published by ESG (www.electrochemsci.org). This article is an open access article distributed under the terms and conditions of the Creative Commons Attribution license (<http://creativecommons.org/licenses/by/4.0/>).